NUMERICAL COMPARISON OF STEADY DISTURBANCES IN THE WAKE OF PERIODIC BLOW–SUCTION AND ROUGHNESS ELEMENTS

P.V. Chuvakhov,[*,**] S.V. Alexandrov,[*,**] E.A. Alexandrova[*,**]
[*]Central Aerohydrodinamic Institute (TsAGI)
[**]Moscow Institute of Physics and Technology (MIPT)

Keywords: *roughness, blow–suction, compression ramp, cfd, Görtler vortices*

Abstract

Numerical simulations of the effect of Görtler-like vortices is investigated for a laminar Mach 8 15° compression corner flow for Reynolds number $Re_{\infty,L}=3.71\times10^5$ based on flat plate length. Two ways of seeding the vortices of various intensity ahead of separation bubble are considered. The first deals with periodic blow–suction with controllable spanwise amplitude of the normal-to-wall mass rate. The second deals with periodic cylindrical roughness elements of various heights. Both ways are compared in terms of flow patterns and surface heat flux.

1 Introduction

Investigation of high-speed compression ramp flows is of practical and fundamental interest in the context of the development of thermal protection systems for control surfaces (flaps, elevons). Flow reattachment at the inclined surface (also called as ramp or wedge) may lead to excessive heat flux regions and form favorable conditions for Görtler vortices to occur. Such vortices are seeded by surface irregularities that also determine the vortices intensity. Being amplified in the reattachment region, the vortices may result in considerable variations of heat flux with amplitudes up to 100% of its spanwise-averaged value (see, e.g., [1]). The presence of vortices may also increase the mean value of heat flux, which is commonly connected to transitional state of the reattachment flow [2]. However, numerical investigations [1, 3] showed that this may happen in a purely laminar flow. Though different in nature, similar effect was observed in direct numerical simulation [4] of fundamental breakdown on Mach 6 cone where regular streamwise streaks occurred because of nonlinear processes and caused sharp increase of heat flux before the transition to turbulence took over.

To predict the effect of Görtler vortices on heat flux on the basis of Navier–Stokes equations one should somehow excite steady disturbances upstream the reattachment where the disturbances amplify. To this effect, there are three principle ways. The first relies on the uncontrolled numerical errors that appear because of imperfections of numerical schemes or grids, etc. Their being uncontrollable is the main shortcoming of this approach if variation of disturbance level is required. The second way is to put disturbances directly into the base flow by using volume (e.g., thermal spots) of boundary conditions (blow–suction of fluid). This way is widely used for direct numerical simulation of laminar-turbulent transition. The later way is to directly model the surface roughness elements, which is rather difficult to implement numerically.

In recent experiments [5, 6] Görtler-like vortices were seeded by a periodic rake of cylindrical roughness elements located upstream of the separation bubble. The geometry of the rake (diameter, spacing and height) were controlled. The flow regime was assessed as near-laminar or transitional. The experiments showed that regular streamwise Görtler-like vortices may lead to increase of spanwise-

averaged value and spanwise variations of heat flux even in the case when the flow is close to laminar.

However, it is difficult to model blow–suction actuator in experiments. It is also time-consuming to simulate a flow past roughness elements numerically.

The purpose of the present study is to extend the above-mentioned numerical and experimental findings [1, 3, 5, 6] in order to couple the effects of streamwise vortices of various intensity seeded by cylindrical roughness elements or via blow–suction ahead of the separation bubble. The former approach assumes variation of the height of a periodic roughness rake. The latter assumes variation of the amplitude of spanwise blow–suction mass rate. The both approach are compared in terms of their effect on the flow and surface heat flux.

2 Numerical problem formulation

The numerical problem formulation corresponds to that in [1, 3] with extension for modeling of roughness-induced disturbances. Below stated are the numerical conditions for which Görtler vortices have been observed experimentally [1].

A hypersonic Mach 8 compression corner flow is investigated in the framework of perfect gas at Reynolds number $\mathrm{Re}_{\infty,L} = 3.71 \times 10^5$ based on the flat plate length $L = 50$ mm; stagnation temperature $T_0 = 754$ K; wall-to-stagnation temperature ratio $T_w/T_0 \approx 0.39$. The plate leading edge is sharp. The ramp is inclined at 15° with respect to the plate surface. Dynamic coefficient of molecular viscosity is in accord with Sutherland's law with the constant $T_{SUTH} = 110.4$ K.

Hereafter all variables are considered in usual non-dimensional form. All coordinates (x, y, z) are scaled with respect to L; velocity components (u, v, w) and temperature T are scaled to their free-stream values u_∞^* and T_∞^*, respectively; pressure $p = p^*/\rho_\infty^* u_\infty^{*2}$; time $t = t^* u_\infty^*/L$.

The computational domain is a rectangular box with streamwise x, spanwise z and normal-to-plate y directions. The width in z equals the wave length of naturally induced Görtler vortices, $z_{\min} = 0$, $z_{\max} = \lambda = 0.062$,which has been observed in experiments [1]. Thus, the only vortex pair is simulated. The verification of this approach is given in [3]. The streamwise length of computational domain equals to two. The upper boundary of the domain is above all the features of compression corner flow and thereby at free-stream conditions.

Boundary conditions are usual for short-time experiments. The surface is supposed to be isothermal and no-slip: $T_w = 5.36$, $(u, v, w)_w = (0,0,0)$. At the inflow boundary, Dirichlet-type free stream boundary conditions are imposed: $(u, v, w)_\infty = (1,0,0)$, $p_\infty = 1/(\gamma M^2)$, $T_\infty = 1$, $\gamma = 1.4$. At the outflow boundary, all dependent variables u, v, w, p, T are linearly extrapolated from the interior. Spanwise periodicity is imposed on the solution at side (z) boundaries.

All simulations are performed using an in-house software HSFlow that implements a quasimonotonic Godunov-type numerical scheme of second order in space and time [7]. All flow fields are obtained by advancing the initially free-stream flow to its steady state. The steady state is supposed to be attained when relative change of all dependent variables does not exceed 10^{-6} over the characteristic flow time $t_c = 1$.

The nominally two dimensional flow is perturbed ahead of the separation bubble either by using a periodic blow-suction actuator or by a rake of cylindrical roughness elements placed at $x_0 = 0.1$. In both cases, the numerical grid is clustered toward the leading edge and to the wall to ensure about 150 grid points at the perturbation station.

Analysis focuses on distributions of heat flux coefficient that is further referred to as the Stanton number (St):

$$\mathrm{St} = \frac{\mu_w}{\mathrm{Re}_{\infty,\mathrm{L}}\,\mathrm{Pr}(T_0 - T_w)}\left(\frac{dT}{d\vec{n}}\right)_w \qquad (2)$$

The vortices give rise to spanwise variations of heat flux. Thus, the z-averaged distribution of St is considered, $\mathrm{St}_{zAvg}(x)$.

Figure 1 illustrates the unperturbed steady-state solution. A bow shock wave due to viscous-invisid interaction near the leading edge is hardly visible in the slice $z = const$ where Mach field is shown. All the slices $x = const$ show the u field: $x = 0.49$ (1), 0.7 (2), 1.3 (3),

1.68 (4), 1.78 (5), 1.88 (6), and 1.98 (7). Laminar boundary layer develops to $x_{sep} \approx 0.5$ and separates from the flat plate to proceed as a mixing layer and eventually reattach at the ramp surface at $x_{rea} \approx 1.4$. The corresponding shocks of separation and reattachment arise. They combine near the slice 6 close to the outflow boundary of the computational domain. The hypersonic flow turns at those shocks. However, there is a region near the reattachment (slice 3) with highly curved streamlines where a set of compression waves have not yet combine to form the reattachment shock. It is this region that the Görtler vortices are amplified most.

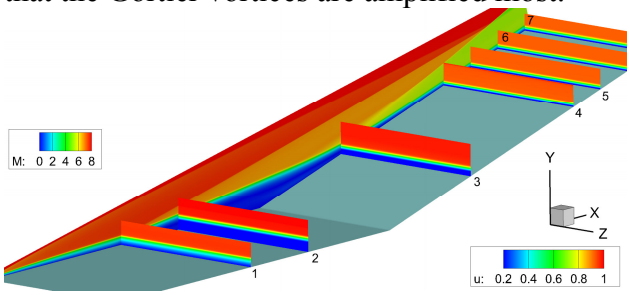

Fig. 1. Unperturbed steady-state solution.

2.1 Blow–suction actuator

A multiblock numerical grid of about 4.2 millions nodes, $600 \times 300 \times 23$, with structured Cartesian topology is used for simulations with blow–suction actuator. The actuator produced small steady disturbances ahead of the separation bubble:

$$(\rho v)'_w = \varepsilon \sin\left(\pi \frac{x-x_0}{x_1-x_0}\right) \sin\left(2\pi \frac{z-z_{\min}}{z_{\max}-z_{\min}}\right), \quad (1)$$

with $x_1 = 0.13$. The reader is referred to the work [3] for details including verification.

The value of actuator intensity ε varies among 0.001, 0.002, 0.005, 0.007, 0.01, 0.02 and 0.05.

2.2 Rake of roughness elements

Numerical grids of unstructured topology contain about six millions nodes, $800 \times 330 \times 23$. The roughness element is a cylinder of diameter $d = 0.02$ centered at side boundaries (see Fig. 2). The streamwise cylinder edge is located at x_0. The height of the cylinder varies among $k/\delta_k = 0.1, 0.3, 0.4, 0.5, 0.7, 1.0$, where δ_k is a boundary layer (BL) thickness, $u(\delta_k) = 0.99$. Each case has its own multiblock structured hexahedral grid. The reference grid corresponds to the case 1.0. It has two half 'O' grid regions in $x - z$ plane near and above the roughness elements. Other grids are obtained by adding 'O' grid blocks that fill the space between the top surface of the roughness and that for current value of k/δ_k.

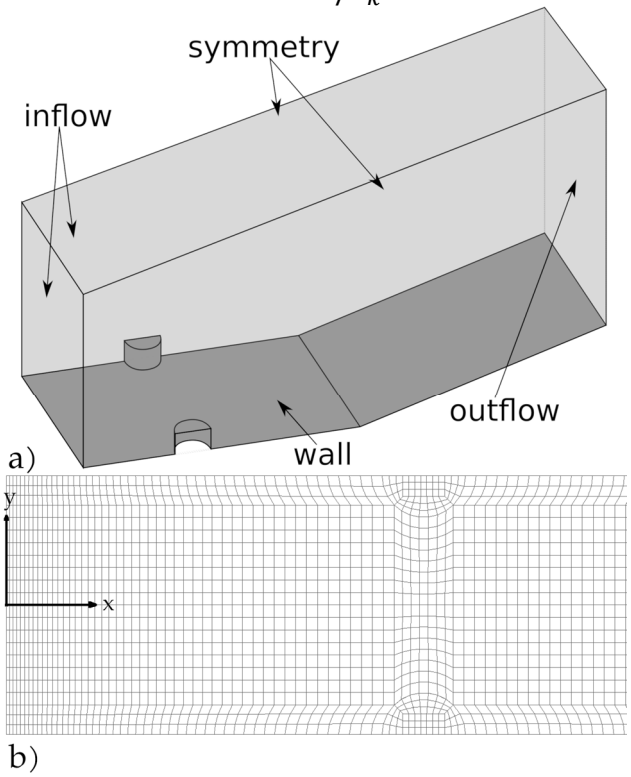

Fig. 2. Schematic of grid with roughness (not in scale).

To reduce computational time for every roughness case the unperturbed steady-state flow field (no roughness) is mapped to the grid with roughness using linear interpolation. The resultant is used as an initial approximation at $t = 0$, with the roughness element emerged into the unperturbed boundary layer. Typical solution convergence time is from 50 to 100 depending on the case. The front part of steady-state flow fields is eventually left out to ease the further analysis using the single-block format.

The computations of roughness-induced disturbances are time-consuming and make grid convergence study difficult to carry out. Besides the verification study of [3] for blow–suction case, further effort is to be put to the resolution of roughness elements, that is the matter of future work.

3 Results

3.1 General flow fields

Figure 3 illustrates the general isometric view of the flow fields with perturbing elements (blow–suction or roughness). Weak perturbation (a, b) affect marginally the base flow, as would be expected. Though hardly detectable above the separation bubble, the seeded disturbances produce striation pattern behind the reattachment, which is visible as a slight distortion of the streamlines. These streamlines are evaluated as a set of streamlines passing through the line $x = 0.4, y = y_w + 0.01$ (ahead of the separation bubble and slice 1). The boundary layer is slightly disturbed there.

Increasing the seeding intensity (c, d) leads to the stronger effect behind the reattachment. The small disturbances become slightly visible above the separation bubble. They twist to Görtler-like streamwise vortices behind slice 3.

Further increase of the seeding intensity (e, f) affects considerably the separation bubble in the case of roughness rake – the bubble shrinks. This has an effect on the vortex structure which appear earlier upstream in comparison with the case of blow and suction, where the separation does not seem to react to the upstream forcing.

Due to the vortex motion, the low-pressure fluid lifts up from the wall to the outer flow, while the high-pressure fluid is entrained to the boundary layer. Sufficiently intense vortices form the so-called mushroom structures behind the reattachment. They lift up progressively downstream and slowly attenuate.

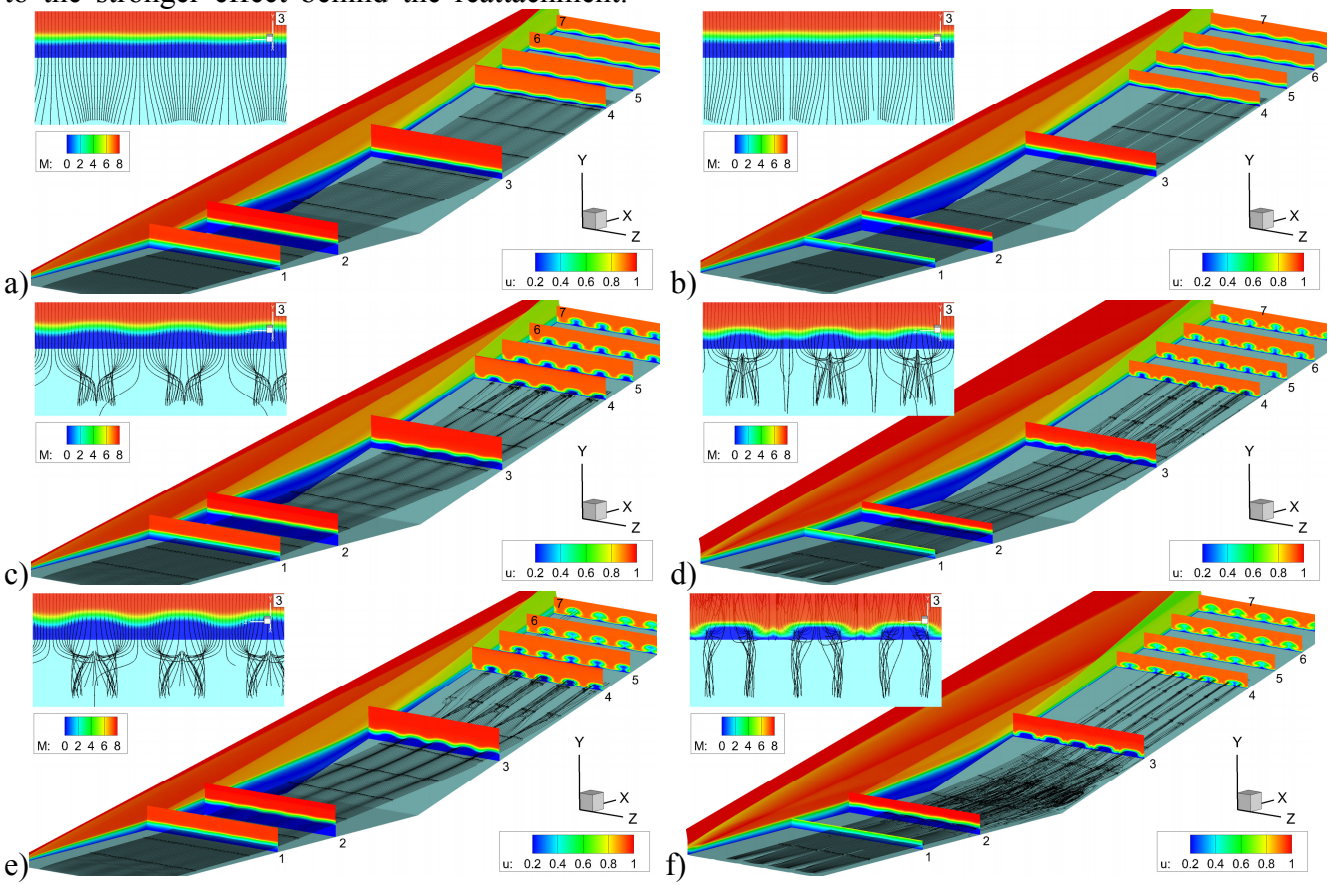

Fig. 3. Perturbed solutions. Blow–suction (left) and roughness-induced (right) Görtler-like vortices.
Stations 1–7 correspond to Fig. 1. Slice 3 is additionally shown from the viewpoint of slice 4. Lines denote streamlines.
$\varepsilon \times 10^3 = 1(a), 5(c), 10(e)$. $k/\delta_k = 0.1(b), 0.5(d), 0.7(f)$.

3.2 Separation bubble behavior

Consider the behavior of separation bubble (see Fig. 4). Separation and reattachment stations are obtained as the zeroes of the z-averaged distributions of skin friction coefficient:

$$C_f = \frac{2}{Re_{\infty,L}} \times \left(\mu \frac{du}{dy}\right)_w . \qquad (2)$$

The blow–suction affects marginally the sizes of the bubble for $\varepsilon < 0.01$. Higher values of ε lead to reducing the reattachment station where Görtler vortices gain their strength, while the reaction of the separation station is negligible. Quite different reversal behavior is observed in the case of roughness seeding. The separation first increases considerably at $k/\delta_k = 0.3$ and then starts decreasing monotonically as k/δ_k rises. Similar reversal behavior of the separation bubble was observed in schlieren experiments with cylindrical roughness rake of controllable height [5, 6] at close-to-present flow conditions. The final separation size in the case of blow–suction is about two times larger than that in the case of roughness.

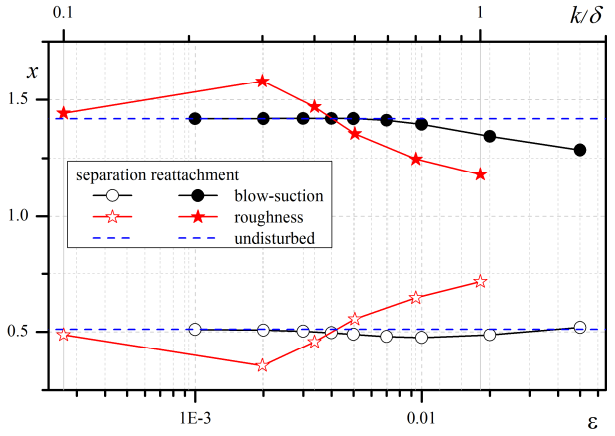

Fig. 4. Separation and reattachment stations. $k/\delta_k \in [0.092, 2.0]$; $\varepsilon \in [2.25 \times 10^{-4}, 0.065]$. The hinge line at $x = 1$.

This above observations point to the fact that the two ways of seeding the streamwise vortices cannot easily substitute one by the other neither in computations nor in experiments.

3.3 Heat flux at reattachment

Figures 5 and 6 illustrate the streamwise distribution of spanwise-averaged St number, $\mathrm{St}_{zAvg}(x)$, for the blow–suction and roughness seeding elements, respectively.

The blow–suction tends to increase the z-averaged heat flux behind the reattachment. The maximum of $\mathrm{St}_{zAvg}(x)$ marked with white circles follows smoothly downstream and then upstream with the value of $\mathrm{St}_{zAvg,\max}$ rising as the value of ε increases.

The behavior of $\mathrm{St}_{zAvg}(x)$ curves for the roughness case differs noticeably (Fig. 6). The reversal behavior noted above (see. Fig. 4) is apparent here. A rather tall roughness rake may penetrate to the supersonic part of the boundary layer and give rise to the entropy effect, i.e. drop in local Reynolds and Mach numbers due to formation of highly curved bow-shock waves near the roughness element. This effect is known to result in reversal behavior of separation bubble that occurs in compression corner flows behind blunt leading edge as the bluntness size increases [8]. The reversal behavior observed in the present work for the case of roughness (see Fig. 4, 5) is supposed to be also attributed to the entropy effect.

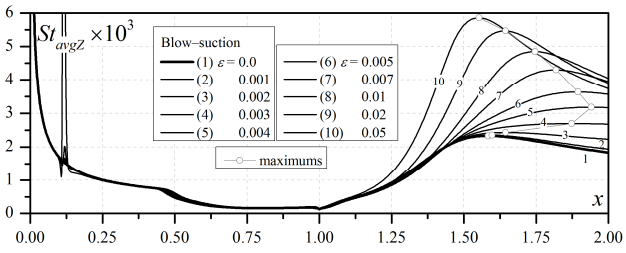

Fig. 5. Distribution of $\mathrm{St}_{zAvg}(x)$, blow–suction seeding.

The smallest considered roughness reduces slightly the z-averaged level of heat flux at the reattachment region. The trace of maximums of $\mathrm{St}_{zAvg}(x)$ (Fig. 6) is not as smooth as for the case of blow–suction (Fig. 5), though it again moves first downstream and then come upstream as the vortices become stronger and separation bubble shrinks. Note that the maximum for $k/\delta_k = 0.3$ is at the outflow boundary and may be underestimated. This does not influence the corresponding station of reattachment.

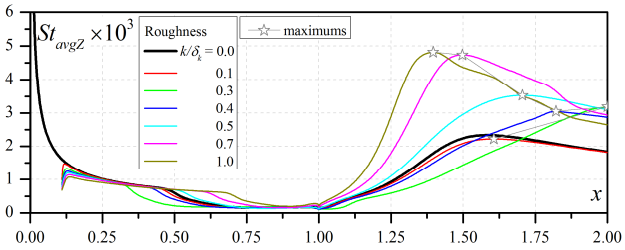

Fig. 6. Distribution of $\mathrm{St}_{zAvg}(x)$, roughness seeding.

Consider Fig. 7 that summarizes the results of Figs. 6 and 7 and also provides the levels of spanwise variation of St at the station of maximum $\mathrm{St}_{zAvg}(x)$. The top and the bottom axis scales are chosen to nearly fit to each other. This fitting has become a basis for the cross-comparison of flow patterns (Fig. 3) and for the choice of the scales for Figs. 5, 6.

The spanwise variations seem to follow the maximum value of St_{zAvg}. Noticeable variation is present even in the case of the smallest perturbations considered, where $\mathrm{St}_{zAvg,\max}$ is close to the unperturbed flow. The reversal trend discussed above is also reflected in Fig. 7 at $k/\delta_k = 0.3$. Nevertheless, the variations look similar for small perturbations: $k/\delta_k \le 0.5$ and $\varepsilon \le 5 \times 10^{-3}$. Both blow–suction and roughness seeding ways show the saturating trends as the perturbation intensity increases. However, the saturation levels do not appear to coincide. This also points to the fact that the two seeding approaches are different in nature and cannot be substituted one by the other, in particular for high level of perturbations.

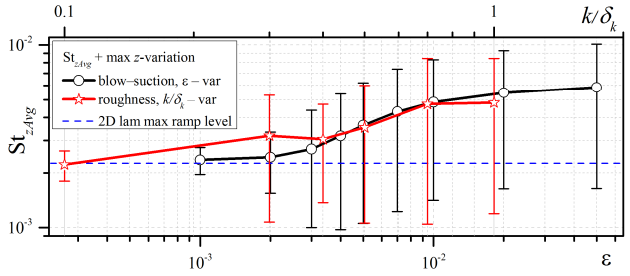

Fig. 7. Summary: maximums of $\mathrm{St}_{zAvg}(x)$ and spanwise variation of St at the maximum stations.

4 Conclusion

Numerical simulations of the effect of Görtler-like vortices is investigated for a laminar Mach 8 15° compression ramp flow for Reynolds number $\mathrm{Re}_{\infty,L}=3.71\times10^5$ based on flat plate length. Two ways of seeding the vortices of various intensity ahead of separation bubble are considered. The first deals with periodic blow–suction with controllable spanwise amplitude of mass rate. The second deals with periodic cylindrical roughness elements of various heights.

The computations confirm the rise of spanwise variations and spanwise-averaged value of heat flux at reattachment in the presence of sufficiently intense streamwise vortices. The effect saturates as the intensity of perturbation increases.

The both ways are capable of producing streamwise vortices of various intensity at reattachment. However, the separation region is sensitive to the height of a roughness rake. It increases at low roughness heights and shrinks at tall roughness height. This may be attributed to the entropy layer effect. Much smaller effect is observed for the way of blow–suction. Thus, maximum spanwise variation and spanwise-averaged value of heat flux occur at different location depending on the way of seeding. This makes it difficult to substitute one way by the other either in computations or in experiments.

Although this work captures the general features of a compression corner flow with seeding elements, additional verification effort is still required.

Acknowledgements

The work has been supported by Russian foundation for basic research (project no. 17-08-00567). Numerical simulations have been carried out using computing resources of the federal collective usage center Complex for Simulation and Data Processing for Mega-science Facilities at NRC “Kurchatov Institute”, http://ckp.nrcki.ru/, and high-performance computing resources of Moscow Institute of Physics and Technology.

References

[1] Chuvakhov P.V., Borovoy V.Ya., Egorov I.V., Radchenko V.N., Olivier H, and Roghelia A. Effect of Small Bluntness on Formation of Görtler Vortices in a Supersonic Compression Corner Flow. *Journal*

of Applied Mechanics and Technical Physics, Vol. 58, No. 6, pp. 975–989, 2017.

[2] Simeonides G. and Haase W. Experimental and Computational Investigations of Hypersonic Flow about Compression Ramps. *J. Fluid Mech.*, Vol. 283, No. 1, pp. 17–42, 1995.

[3] Chuvakhov P.V., Egorov I.V., Olivier H., and Roghelia A. Joint Influence of High Entropy Layer and Goertler Vortices on Heat Transfer in Supersonic Compression Ramp Flow. *Computational Thermal Sciences: An International Journal*, Vol. 8, No. 6, pp. 543–553, 2016.

[4] Sivasubramanian J. and Fasel H.F. Direct Numerical Simulation of Transition in a sharp cone boundary layer at Mach 6: fundamental breakdown. *J. Fluid Mech.*, Vol. 768, pp. 175–218, 2015.

[5] Chuvakhov P.V., Radchenko V.N., and Alexandrova E.A. Controlled experiment on Goertler vortices of various intensity and heat transfer in a hypersonic compression corner flow. *19th International conference on the methods of aerophysical research (ICMAR 2018)*, Novosibirsk, Russia, pp. 1–10, 2018.

[6] Chuvakhov P.V., Radchenko V.N., Alexandrova E.A., and Borovoy V.Ya. Effect of controlled periodic roughness on Goertler vortices in hypersonic compression ramp flow. *Proc. of 31th Congress of the International Council of the Aeronautical Sciences (ICAS 2018),* Belo Orizontie, Brasil, pp. 1–9, 2018.

[7] Egorov I.V. and Novikov A.V. Direct numerical simulation of laminar–turbulent flow over a flat plate at hypersonic flow speeds. *Computational Mathematics and Mathematical Physics*, Vol. 56, No. 6, pp. 1048–1064, 2016.

[8] Holden M.S. Boundary-layer displacement and leading-edge bluntness effects on attached and separated laminar boundary layers in a compression corner. II. Experimental study. *AIAA J.*, Vol. 9, No. 1, pp. 84–93, 1971.

Contact Author Email Address

mailto:pavel_chuvahov@mail.ru

Copyright Statement